The tuber-specific StbHLH93 gene regulates proplastid-to-amyloplast development during stolon swelling in potato

Article *in* New Phytologist · December 2023

DOI: 10.1111/nph.19426

11 authors, including:

Sun Sifan
Yunnan University
9 PUBLICATIONS **101** CITATIONS

SEE PROFILE

Research

New Phytologist

The tuber-specific *StbHLH93* gene regulates proplastid-to-amyloplast development during stolon swelling in potato

Rui Yang[1]*, Yuan Sun[1]*, Xiaoling Zhu[1]*, Baozhen Jiao[1], Sifan Sun[1], Yun Chen[1], Lizhu Li[1], Xue Wang[1], Qian Zeng[1], Qiqi Liang[1] and Binquan Huang[1,2]

[1]State Key Laboratory for Conservation and Utilization of Bio-Resources in Yunnan, School of Agriculture, Yunnan University, Kunming, 650500, China; [2]Southwest United Graduate School, Kunming, 650500, China

Author for correspondence:
Binquan Huang
Email: binquanh@ynu.edu.cn

Received: *24 July 2023*
Accepted: *5 November 2023*

New Phytologist (2024) **241:** 1676–1689
doi: 10.1111/nph.19426

Key words: amyloplast development, potato, *StbHLH93*, stolon swelling, tuber-specific transcription factor.

Summary

- In potato, stolon swelling is a complex and highly regulated process, and much more work is needed to fully understand the underlying mechanisms.
- We identified a novel tuber-specific basic helix–loop–helix (bHLH) transcription factor, *StbHLH93*, based on the high-resolution transcriptome of potato tuber development.
- *StbHLH93* is predominantly expressed in the subapical and perimedullary region of the stolon and developing tubers. Knockdown of *StbHLH93* significantly decreased tuber number and size, resulting from suppression of stolon swelling. Furthermore, we found that StbHLH93 directly binds to the plastid protein import system gene *TIC56* promoter, activates its expression, and is involved in proplastid-to-amyloplast development during the stolon-to-tuber transition. Knockdown of the target *TIC56* gene resulted in similarly problematic amyloplast biogenesis and tuberization.
- Taken together, *StbHLH93* functions in the differentiation of proplastids to regulate stolon swelling. This study highlights the critical role of proplastid-to-amyloplast interconversion during potato tuberization.

Introduction

Potato (*Solanum tuberosum*) is the most important nongrain food crop species in the world. Tuber number and size are key yield components of potatoes; however, few potato genes and pathways impacting tuber formation have been reported. Thus, much work is needed to identify key genes related to tuber development and elucidate the underlying molecular mechanisms.

Potato tuber formation is mainly divided into three stages: (1) stolon induction, (2) stolon-to-tuber transition, and (3) tuber initiation and growth (Zierer *et al.*, 2021). Under inductive photoperiod conditions, the phenotypic indication for developmental transitions of stolon is the cessation of longitudinal growth, followed by visible straightening of the stolon apical hook (Xu *et al.*, 1998; Abelenda *et al.*, 2019; Zierer *et al.*, 2021). During the initial stolon-to-tuber transition in the subapical region, the central pith tissue began to extend, resulting in arc-shaped vascular bundles, and the extension of the outer cortex region was limited. Tuber growth is mostly driven by expansion and radial cell division within the perimedullary zone. After the diameter of tubers has grown to *c.* 8 mm, tuber enlargement continues via increased thickness of the perimedullary zone until the tuber reaches its final size (Xu *et al.*, 1998; Zierer *et al.*, 2021). These changes in cell division and extension are accompanied by a switch in the developmental program of the stolon subapical meristem cells to a tuber fate (Kondhare *et al.*, 2021a).

Stolon-to-tuber interconversion is one of the most important dynamic processes in tuber formation. Various genes, such as the tuberigen *SELF PRUNING 6A* (*StSP6A*; Navarro *et al.*, 2011), *PHYTOCHROME B* (*StPHYB*; Jackson *et al.*, 1998), *CYCLING DOF FACTOR 1* (*StCDF1*; Kloosterman *et al.*, 2013), *BRANCHED 1b* (*BRC1b*; Nicolas *et al.*, 2022), *ABI5-LIKE 1* (*StABL1*; Jing *et al.*, 2022), *StSWEET11* (Abelenda *et al.*, 2019), and *SUCROSE TRANSPORTER 4* (*StSUT4*; Chincinska *et al.*, 2013), have been identified as key components involved in the regulation of tuberization, which indicates that the tuber formation in potato is controlled by multiple signals. Cultivated potatoes originate in the Andes Mountains, and most wild potato species require short-day (SD) lengths and cool temperatures for tuberization; thus, photoperiod and temperature are the most important factors that influence tuber development (Spooner *et al.*, 2014; Tang *et al.*, 2022). The photoperiod regulates the transport of mobile tuberization signals through the plant to the belowground stolon to trigger axillary meristem development and promote stolon swelling, which occurs through factors such as *StSP6A*, *miR172*, *miR156*, and *BELLRINGER-1 like 5* (*StBEL5*; Martin *et al.*, 2009; Navarro *et al.*, 2011; Lin *et al.*, 2013; Bhogale *et al.*, 2014). Compared with low temperatures, high temperatures delay or even inhibit tuberization by altering the expression of tuberization key-related genes, such as

*These authors contributed equally to this work.

SELF-PRUNING 5G (*StSP5G*), *CONSTANS-LIKE 1* (*StCOL1*), *GIGANTEA* and *StSP6A*, leading to decreased tuber number and size (Hancock *et al.*, 2014; Singh *et al.*, 2015; Park *et al.*, 2022). In addition, endogenous phytohormones are known to synergistically regulate stolon-to-tuber transition and tuber development. In general, cytokinins and auxins are positive regulators of the stolon-to-tuber transition, while strigolactones and gibberellins are negative regulators of this transition (Roumeliotis *et al.*, 2012; Abelenda & Prat, 2013; Kondhare *et al.*, 2021b); and a tightly balanced auxin-strigolactone interaction is important for the formation of tubers (Hayward *et al.*, 2009; Pasare *et al.*, 2013).

Amyloplast, which is derived from proplastids found within dividing cells of apical meristems, is an organelle found in storage organs and is responsible for starch biosynthesis and storage (Sakamoto *et al.*, 2008; Jarvis & Lopez-Juez, 2013). The differentiation of proplastids into amyloplasts is an important process during stolon swelling, which require the import of thousands of nucleus-encoded proteins from the cytosol, initiated by multiprotein TRANSLOCON complexes in the plastid envelope membrane (Brosch *et al.*, 2007; Stensballe *et al.*, 2008; Jarvis & Lopez-Juez, 2013; Thomson *et al.*, 2020; Zierer *et al.*, 2021). This protein transportation is catalyzed by TRANSLOCON complexes in the outer (TOC) and inner (TIC) chloroplast envelope membrane (Thomson *et al.*, 2020). The TOC complex mainly consists of Toc33, Toc75, and Toc159, and the TIC complex consists of Tic214, Tic100, Tic56, Tic20, and Tic21 (Jarvis & Lopez-Juez, 2013). Plastids are not limited to the production of metabolites but can also determine extraplastidic functions and affect numerous aspects of plant growth and development, such as embryogenesis, leaf development, and fruit ripening (Kode *et al.*, 2005; Inaba & Ito-Inaba, 2010; Romani *et al.*, 2012; Leister & Kleine, 2016; Duan *et al.*, 2020).

In this study, we performed a comprehensive RNA sequencing (RNA-Seq) transcriptome study of tuber development and identified a new tuber-specific transcription factor (TF), *StbHLH93*. We showed that, by regulating proplastid-to-amyloplast interconversion, *StbHLH93* plays an important role in potato tuberization, thus reflecting its critical role in proplastid-to-amyloplast interconversion during potato tuberization.

Materials and Methods

Plant material and growth conditions

Potato plants (*Solanum tuberosum* L.) were propagated *in vitro* using single-node stem on Murashige-Skoog medium supplemented with 3% (w/v) sucrose for 2 wk under long-day (LD; 16-h : 8-h, light : dark) conditions at 22°C. The plants were then transferred to the soil and maintained in a climate chamber for 6 wk under LD conditions. After 6 wk under LD, plants were transplanted into plastic pots with a diameter of 25 cm (one plant per pot) in a growth room with a SD photoperiod (16 h : 8 h, light : dark) at 20 ± 2°C and were managed to ensure normal growth. The noninduced stolon tips used for phenotypic or expression analysis (qPCR or RNA-Seq) were harvested 3–4 h after the SD began, and stolon tips and developing tubers (stages 2–8) were harvested for 25 d after the switch to SD conditions. Plants at all stages were harvested 3–4 h after they were transferred to the light. For the luciferase (LUC) assays, *Nicotiana benthamiana* plants were grown at the glasshouse under similar conditions.

Plant phenotyping

For potato yield analyses, underground parts of soil-grown plants were harvested for 25 d after switching to SD conditions, and tuber number and weight were scored. Data were collected from 10 to 12 plants for each of the three independent transformation events. To analyze the numbers of stolon and swollen stolon, stolon tips were investigated from wild-type (WT) and transgenic plants at 0, 5, 7, 9, 15, and 20 d after the plants were transferred to soil and switched to SD conditions. In this study, all statistics were based on plants from three different transformation events, specifically, at least five individual plants for each event were used for the statistical analyses.

RNA-Seq analysis

The plant material was obtained from tetraploid potato cultivar *S. tuberosum* L. cv Atlantic, grown in a controlled environment under LD conditions and subsequently switched to SD conditions to promote synchronous tuberization. Potato stolons and tubers were collected at eight developmental time points, encompassing the entire process of tuber development, as described previously (Kloosterman *et al.*, 2005). For each stage, 10–15 stolons or tubers were pooled for each of the four biological replicates for RNA extraction. These samples were immediately placed in liquid nitrogen and stored at −80°C. Total RNA was extracted using the TRIzol reagent (Invitrogen). RNA-Seq was performed by staff at the Beijing Genomics Institute (BGI). The DM1-3516 R44 reference genome sequence (SolTub_3.0; Potato Genome Sequencing Consortium, 2011) was downloaded from https://www.ncbi.nlm.nih.gov/assembly.

Gene co-expression and functional enrichment analysis

MeV (v.4.9) software with the k-means method was used for co-expression analysis of the samples collected at eight different time points. The normalized expression values of the genes were calculated by dividing their expression levels at different time points by their maximum observed FPKM values.

Gene Ontology (GO) enrichment analysis maps all candidate genes to each entry in the GO database (http://www.geneontology.org/), calculates the number of genes per entry, and then applies a hypergeometric test to identify the GO function that was significantly enriched in candidate genes compared with all background genes of the species. Kyoto Encyclopedia of Genes and Genomes (KEGG) pathway enrichment analysis was performed using the same methodology as the GO functional enrichment analysis.

Gene regulatory network inference and identification of stolon- and tuber-specific gene expression

We inferred the gene regulatory network (GRN) that connects TFs with their potential target genes using the context likelihood of relatedness algorithm method reported previously (Faith *et al.*, 2007; Xiong *et al.*, 2017). The mutual information (MI) for calculating the expression similarity between the expression levels of TF and gene pairs was calculated using R software (https://bioconductor.org/packages/release/bioc/html).

To identify stolon- and tuber-specific genes, we used the transcriptomic data set of *S. tuberosum* group Tuberosum RH89-039-16, which included data for the root, stem, leaf, petiole, flower, stamen, stolon, and tuber tissues. This analysis was performed as described previously (Yi *et al.*, 2019).

Real-time qPCR (RT–qPCR)

Total RNA was extracted from the frozen samples using the MiniBEST Plant RNA Extraction Kit (Takara, Shiga, Japan). We used 1 μg of total RNA for reverse transcription with Rever-Tra Ace qPCR RT Master Mix with gDNA Remover (Toyobo, Osaka, Japan) following the manufacturer's instructions. The complementary DNA (cDNA) was diluted five times before performing RT-qPCR. GoTaq qPCR Master Mix (Promega) and an Applied Biosystems 7500 real-time PCR system were used to perform RT-qPCR. The primers used are listed in Supporting Information Table S1. *StACTIN8* was used as a reference gene (Navarro *et al.*, 2011; Nicolas *et al.*, 2022). Three technical replicates were used for each of the three biological replicates. The relative gene expression was calculated using the $2^{-\Delta\Delta C_t}$ method.

Morphological and cellular analyses

Stolons, swollen stolons, and young tubers were gently excised and fixed in formaldehyde-acetic acid-ethanol (FAA) solution (70% ethanol : formaldehyde : acetic acid, 9 : 1 : 1). For histological analysis, the fixed samples were dehydrated in a graded ethanol series (50–60–75–80–95–100–100%). The samples were then passed through a xylene–ethanol series and embedded in Paraplast, with six changes in Paraplast. The blocks were sectioned into 8 μm slices using a rotary microtome (Leica Biosystems, Buffalo Grove, IL, USA) and subsequently mounted onto slides. The slides were observed under a Leica DM3000 microscope and imaged using a digital camera.

Transmission electron microscopy observations

The cortex region of stolons, swollen stolons, and young tubers was fixed overnight at 4°C using 2.5% glutaraldehyde in 0.1 M PBS (pH 7.2), after which they were washed with 0.1 M PBS (pH 7.2) three times for 7 min. Afterward, the samples were post-fixed with 1% OsO4 for 2 h at 4°C and then washed with ddH_2O three times for 7 min, followed by serial ethanol dehydration and acetone transition for 5 min. They were then embedded in Epon 812 resin and subjected to polymerization at 60°C for 48 h. Serial sections of uniform thickness (800 nm for semithin sections and 60 nm for ultrathin sections) were made using a Leica EM UC7 ultramicrotome. The ultrathin sections were then loaded onto Cu grids and double stained with 2% uranyl acetate and lead citrate before observation under a JEM-1400 Plus transmission electron microscopy (TEM) at 80 kV (Institutional Center for Shared Technologies and Facilities of the Kunming Institute of Zoology, Chinese Academy of Sciences).

In situ hybridization

Stolons, swollen stolons, and young tubers were dissected from the plants and fixed in FAA solution. The samples were then passed through a xylene–ethanol series and embedded in Paraplast, with six changes in Paraplast. The blocks were sectioned into 8 μm slices using a rotary microtome (Leica Biosystems) and mounted onto Poly-Prep slides (Sigma–Aldrich). To generate probes for *StbHLH93*, cDNA-specific fragments were amplified with the primers listed in Table S1 and then cloned into a pEASY-Blunt simple vector (TransGen Biotechnology, Beijing, China). Sense and antisense probes were synthesized with T7 RNA polymerase (Roche Diagnostics, Mannheim, Germany) using a digoxigenin RNA labeling kit (Roche Diagnostics) following the manufacturer's instructions. Nonradioactive *in situ* hybridization was performed according to a previously described method (Yang *et al.*, 2022).

Yeast one-hybrid and luciferase assays

The yeast one-hybrid (Y1H) and LUC assays were performed as described previously (Zhuang *et al.*, 2019). For Y1H assays, *EcoRI* and *SalI* sites were used to insert the promoter region (−1500 bp) of three genes (*TIC56*, *50S ribosomal protein L24*, and *malate dehydrogenase*) fragments into the pLacZi2u vector. Full-length *StbHLH93* was ligated into the *XhoI* and *EcoRI* sites of the GAD vector. The two plasmids were co-transformed into yeast strain EGY48. The cells were plated first onto SD-Ura/−Trp (Clontech, Shiga, Japan) selective media, and positive clones were cultured on a second selective media (SD-Ura/−Trp) supplemented with galactose (20%), raffinose (20%), BU salt (50 ml: 1.95 g Na_2HPO_4, 1.855 g $NaH_2PO_4.2H_2O$), and X-Gal (Sigma–Aldrich). The HY5 TF and *ABI5* promoter sequences from *Arabidopsis* were used as positive controls (Li *et al.*, 2010). For the tobacco transient expression assay, the *proTIC56* was cloned into the pGreenII0800-LUC vector using *BsaI* (Thermo Fisher Scientific), and full-length *StbHLH93* was introduced into the pGreenII62sk vector using *BamHI* and *SalI* (Thermo Fisher Scientific). Five-week-old *N. benthamiana* seedlings were used for transformation as described previously (Zhuang *et al.*, 2019). Fluorescence was measured using a Lumina II instrument (Xenogen, Alameda, CA, USA) and a D-Luciferin Firefly (Gold Biotechnology, St Louis, MO, USA).

SDS–PAGE and immunoblotting

Potato stolon protein extraction was conducted as described previously (Jing *et al.*, 2022). Approximately 200 mg stolon subapical tissue from transgenic and WT plants was used for each sample.

Total protein samples of 40–50 μg were typically analyzed. The potato protein samples and immunoprecipitates were separated on a 10% SDS–PAGE gel and transferred to a polyvinylidene fluoride membrane. Blots were immunodetected using an anti-ZmBt2 (51 kDa), anti-ZmSBE1 (93 kDa), and anti-Actin (43 kDa), followed by incubation with a secondary antibody at a 1 : 5000 dilution (anti-mouse and anti-rabbit HRP-conjugated antibody). Enhanced chemiluminescence detection was performed using SuperSignal West Pico and Femto Substrates (Pierce, Waltham, MA, USA).

Vector construction and potato transformation

All primers used are listed in Table S1. To generate the *StbHLH93*-OX and *StbHLH93*-KD construct, the complete coding sequence and 300-bp unique artificial microRNA (amiRNA) sequences of *StbHLH93* were amplified from tetraploid potato cultivar *S. tuberosum* L. cv Désirée cDNA and DNA, respectively. The purified PCR produacts were inserted into the pART-CAM vector using an In-Fusion® HD Cloning Kit (Takara). This generated the pART-CAM-*StbHLH93* (*StbHLH93*-OX) and pART-CAM-*amiStbHLH93* (*StbHLH93*-KD) vectors. The resulting plasmids were freeze–thaw transformed into *Agrobacterium tumefaciens* strain GV3101, which was then transformed into the Désirée line, as previously described (Millam, 2006).

For the *TIC56*-KD construct, the 2.5 kb promoter of the *StbHLH93* gene was amplified by PCR using DNA from Désirée. The purified PCR products were inserted into the pCAM1300 vector. Next, 300 bp unique cDNA fragment of *TIC56* was amplified from Désirée cDNA and inserted into pCAM1300-*proStbHLH93* to create the pCAM1300-*proStbHLH93::amiTIC56* (*TIC56*-KD) vector. *TIC56*-OX construction and potato transformation were performed using the same methodology as the *StbHLH93*-OX and *StbHLH93*-KD above.

Results

Transcriptomes from different developmental stages of potato tuber were grouped into four clusters

The entire process of potato tuber formation can be divided into three main phases: stolon induction, stolon-to-tuber transition, and tuber initiation and growth (Zierer *et al.*, 2021). Several important genes related to the stolon-to-tuber transition have been identified; however, little is known about the global gene expression network underlying the initiation of stolon swelling. To identify the key genes expressed at specific stages of tuber development, including those unique to tubers, we generated a set of transcriptomic data encompassing the entire process of tuber development (Fig. 1a). In total, 20 545 expressed genes were detected in at least one of the eight samples, including 786 genes that encoded TFs (Table S2). Hierarchical clustering and principal component analysis (PCA) of the eight time series samples showed that the results were in line with those of the previously reported timing of non-induction of the stolon, induction of the stolon, stolon-to-tuber transition, and tuber initiation and growth (Fig. S1a,b).

To further provide insights into the functional transitions during tuber development, all these genes were further classified using a z-score normalized expression heatmap based on the developmental stage during which the major expression transition occurs, and they were grouped into eight co-expression clusters (Fig. 1b). The KEGG database was used to assign the genes to functional categories for each cluster (Fig. S2), and the genes in each cluster corresponded to enriched pathways related to different biological processes. Cluster I was best represented by 3977 expressed genes that were enriched in a few pathways, including the biological processes of plant hormone signal transduction and photosynthesis (Fig. S2). The genes in cluster I might play an important role in the enlargement of stolons under LD conditions; cluster II was best represented by 5445 expressed genes that were enriched in the glutathione metabolism and peroxisomes pathways, which are involved in reactive oxygen species (ROS) biological processes (Fig. S2), indicating that these genes might play roles in stolon development during the transition from LD to SD, as ROS are important light signaling molecules that regulate plant growth and development under different photoperiod conditions. Cluster III consisted of 6011 genes that were enriched in the proteasome, protein export, and ribosome biogenesis pathways, which are related to the biological process of plastid biogenesis. Clusters IV-V were best represented by 3977 expressed genes that were enriched in the fatty acid biosynthesis and starch and sucrose metabolism pathways and were related to the biological process of carbohydrate accumulation (Fig. S2).

Most potato tuber-specific genes are involved in the stolon-to-tuber transition

Tuber traits constitute a key component of potato yield; thus, it is important to identify stolon- and tuber-specific expressed genes and understand their biological functions, further helping to elucidate the underlying regulatory molecular mechanisms of the involvement of these genes in stolon swelling and tuber development. Based on published transcriptomic data sets of potato (Potato Genome Sequencing Consortium, 2011), 782 (including 63 that encode TFs) stolon- and tuber-specific genes were identified (Fig. 1c). Furthermore, combined with our temporal transcriptome data, these specific genes were classified into eight clusters, and remarkably, 63.17% of these genes (494) were grouped into cluster III, showing that genes in this cluster were more highly expressed from stages 1 to 3 and peaked at stage 3. However, they were less highly expressed at later time points (Figs 1b, S3), indicating that genes in cluster III are involved in stolon-to-tuber transition. Essentially, this transition process was accompanied by proplastid-to-amyloplast development (Fig. S4a–i), which was consistent with the results of the functional categories in which genes in cluster III were mainly involved in plastid biogenesis.

To further identify candidate key genes related to the stolon-to-tuber transition, 494 stolon- or tuber-specific genes in cluster III were used for differential expression analysis ($\log_2$ fold change ≥ 1 and False Discovery Rate < 0.05); we found that

New Phytologist

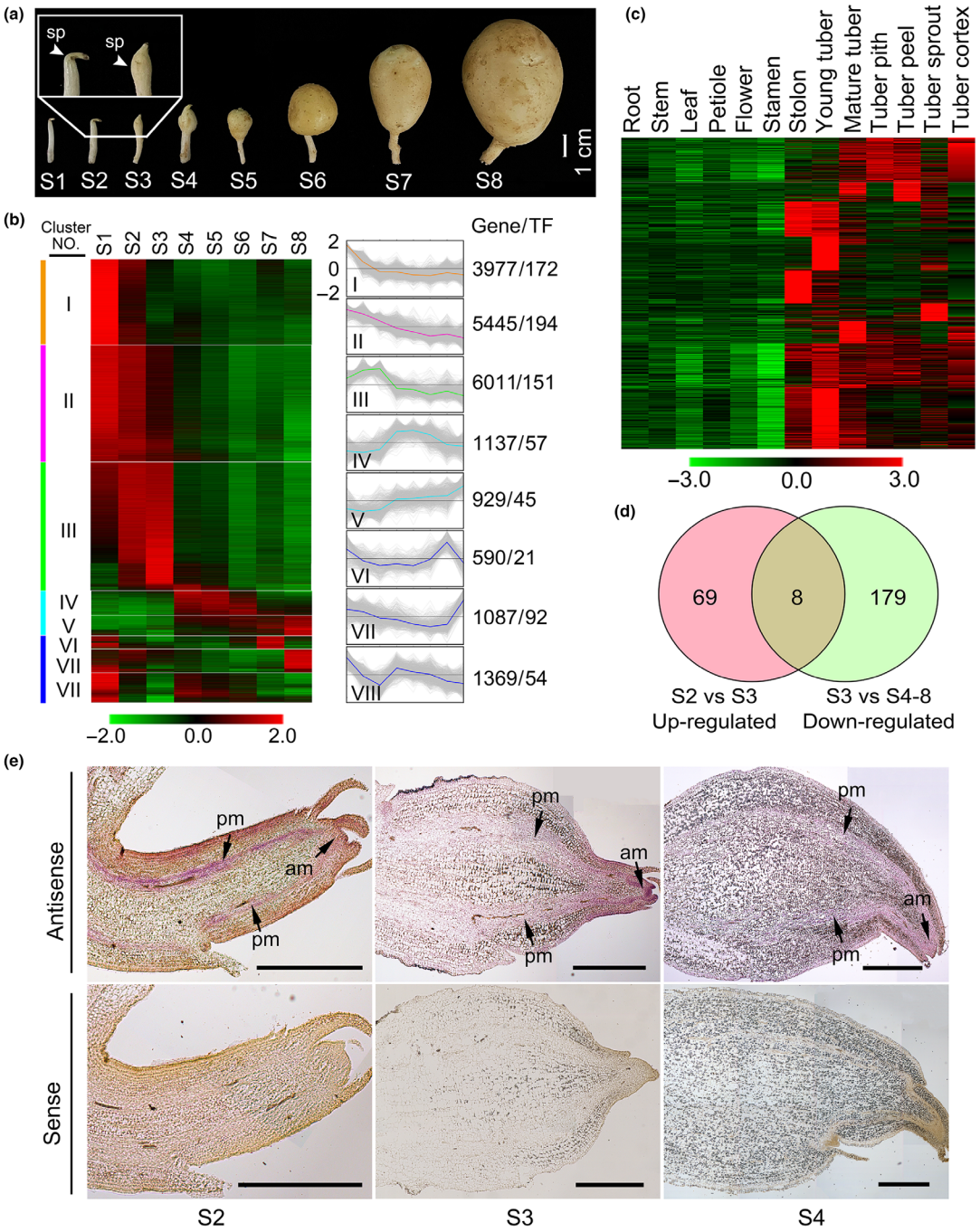

Fig. 1 Identification of transcription factor (TF) associated with stolon swelling in potato. (a) Overview of eight potato tuber developmental stages for 25 d after the plants were transferred from long-day to short-day conditions. (b) Co-expression clusters of genes shared across eight stages of tuber development. For each gene, the normalized expression values (FPKM) were calculated by the maximum value of all gene expression levels at eight different developmental stages. Color scale had been normalized to range from −2 (green) to +2 (red), which represented the high and low expression values, respectively (left). Shown is a graphical (right) representation of cluster gene expression patterns. The lines represent the average expression patterns for all genes in each cluster, and the individual genes are depicted as grey lines. The number of genes and TFs in each cluster is shown on the right. (c) Heatmap showing the expression patterns of stolon- and tuber-specific genes in 13 tissues of *Solanum tuberosum* group Tuberosum RH89-039-16. For each gene, the normalized expression values (FPKM) were calculated by the maximum value of all gene expression levels at eight different developmental stages. Color scale had been normalized to range from −2 (green) to +2 (red), which represented the high and low expression values, respectively. (d) Venn diagram showing the identification of eight differentially expressed genes that are highly expressed at stage 3. (e) *In situ* localization of *StbHLH93* expression in longitudinal and transverse sections during potato developmental. Thin sections (8 μm) through a new tuber/stolon were hybridized with digoxigenin-labeled RNA probes that were synthesized from a full-size *StbHLH93* complementary DNA (cDNA) in either the sense or the antisense orientation. The presence of *StbHLH93* mRNA is indicated by the pink stain under bright-field microscopy. Sense probe is shown as the negative control. Bar, 500 μm. am, apical meristem region; pm, perimedullary region; sp, subapical region.

eight stolon- or tuber-specific genes were specifically upregulated at stage 3 (Fig. 1d), of which only one encoded a TF (*StbHLH93*, *LOC102596640*) that belongs to the basic helix–loop–helix (bHLH) family. qRT-PCR analysis showed that *StbHLH93* was predominantly expressed in the stolon and tuber and confirmed a large increase at the stolon swelling stage during tuber development (Fig. S5). Previous studies have shown that bHLH TFs are primarily involved in cell fate determination and tissue differentiation in plants (Feller *et al.*, 2011; Hao *et al.*, 2021; Zhang *et al.*, 2021). We inferred the GRN that connects TFs with their potential target genes using a previously reported method (Faith *et al.*, 2007; Xiong *et al.*, 2017), and the results showed that *StbHLH93* might be associated with plastid development (Table S3). Furthermore, *in situ* hybridization was performed to detect the exact location of *StbHLH93*, and the results showed that *StbHLH93* transcripts were present in the apical meristem and perimedullary zone with meristematic clusters throughout the stolon-to-tuber transition process, which reflects the important role of *StbHLH93* in stolon swelling (Fig. 1e).

StbHLH93 affects the stolon-to-tuber transition in potato

To further determine the biological function of this bHLH TF in potato tuber formation, we generated transgenic potato plants in the *S. tuberosum* cv Désirée genetic background with altered *StbHLH93* expression. We employed both amiRNA knockdown (KD) and overexpression (OX) driven by the strong 35S promoter. Newly generated transgenic plants were tested by qRT-PCR for changes in gene expression. We selected for analysis three independent KD lines in which *StbHLH93* expression was reduced to *c.* 30% of the WT level, and three independent OX lines in which *StbHLH93* expression was increased more than fivefold relative to WT (Fig. S6a,b). For simplicity, in all subsequent analyses we combined the data from the individual KD and OX lines, as they gave similar results. The *StbHLH93*-KD and *StbHLH93*-OX lines showed significant differences in tuber number and tuber size, whereas there were no significant differences in aboveground phenotypes, including plant height, leaf size, and color, among the *StbHLH93*-OX, *StbHLH93*-KD and the WT plants (Fig. S7a–c). Compared with the WT plants, *StbHLH93*-KD lines presented 43% fewer tubers in total (Fig. 2a,b). In addition, the number of tubers ranging from 15 to 20 g and 20 to 30 g was significantly lower, and there were no tubers > 30 g produced by *StbHLH93*-KD lines (Fig. 2c), which led to a > 50% decrease in tuber yield in transgenic plants compared with WT plants (Fig. 2d). Conversely, *StbHLH93*-OX lines exhibited an enhanced tuber number per plant and an increase in tuber weight, resulting in yield increase compared with the WT (Figs 2b–d, S8).

To further explore whether the decrease in tuber number and weight was related to abnormal stolon swelling or tuber development, we investigated the stolon-to-tuber transition during a period of 25 d after the plants were switched to SD conditions. The results showed that there were no significant differences in stolon numbers among the *StbHLH93*-OX, *StbHLH93*-KD, and WT plants after they were transferred to SD conditions (Fig. 2e). However, we found that the initiation of stolon swelling was delayed in the *StbHLH93*-KD lines, and we did not find swollen stolons at 5 and 7 d after SD growth in the *StbHLH93*-KD lines, whereas the stolon swelling of *StbHLH93*-OX lines was faster compared with WT plants (Fig. 2f). These results suggested that the *StbHLH93* plays an important role in stolon swelling.

StbHLH93 activates the expression of *TIC56* in the tuber of potato

To further understand the regulatory network of the *StbHLH93* gene, GRN analysis revealed three strongly connected genes encoding 50S ribosomal protein L24 (*LOC102582481*), malate dehydrogenase (*LOC102598930*), and Tic56 (TRANSLOCON at the inner envelope membrane of chloroplasts, *LOC102601433*). Functional prediction of these three genes revealed that they were associated with plastid development (Table S3). An *in vitro* Y1H system was used to verify the predicted StbHLH93-target gene regulation. The results showed that only the *TIC56* promoter could be bound by StbHLH93 in yeast, whereas the other two pairs showed no binding affinities compared with those of the positive controls (Figs 3a, S9). Furthermore, four truncated fragments of *proTIC56* (*p1-p4*) were constructed, and the binding affinities of StbHLH93 with the regions of *p1-p4* were examined. The results showed that both *p1::LacZ* and *p2::LacZ* were active, whereas no activity was detected for *p3::LacZ* and *p4::LacZ* (Fig. 3a). To further confirm the binding affinities of StbHLH93 with *proTIC56*, an *in vivo* transient expression assay involving a LUC reporter was used to detect the expression level of *TIC56* by StbHLH93 in *N. benthamiana*. The results showed that, unlike for the control, we observed a strong LUC signal on the injected leaf by using a Lumina II instrument (Fig. S10a), and the LUC-to-Renilla (LUC/REN) ratio was significantly increased by StbHLH93, reflecting a 57.3% increase according to the results of the quantitative analysis of LUC activity (Fig. S10b). Binding affinity tests of StbHLH93-*proTIC56* from both the Y1H and LUC assays indicated that StbHLH93 can bind to the promoter of *TIC56* and activate its expression.

Potato *StbHLH93* regulates proplastid-to-amyloplast transition

Tic56 is a component of the envelope membrane of chloroplasts and a defect that leads to severe developmental defects (Köhler *et al.*, 2015, 2016). To understand the expression pattern of *TIC56* in potatoes, we measured the transcript levels in leaves, roots, flowers, stems, stolons, and tubers. The results showed that *TIC56* was expressed the highest in leaves (Fig. S11a) and that its expression profiles were similar to those of *StbHLH93* in stolons and tubers (Fig. S5). In the *StbHLH93*-KD lines, we found that there was no significant difference in *TIC56* expression levels in the leaves compared with those of the WT plants, whereas the expression level of *TIC56* in stolons or tubers was significantly decreased compared with that in the WT plants (Fig. S11b). To determine whether the expression of other genes related

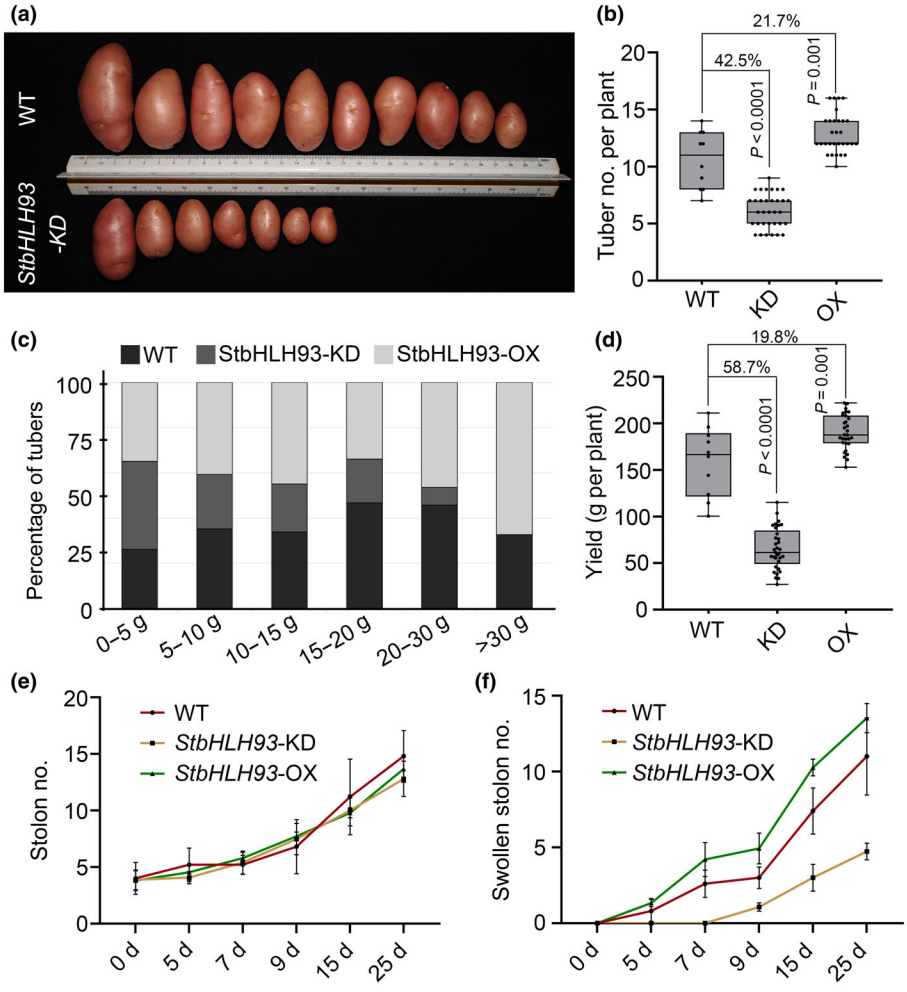

Fig. 2 Phenotypes of potato *StbHLH93*-KD and *StbHLH93*-OX transgenic lines. (a) Tuberization phenotype of a representative *StbHLH93*-KD transgenic plant and wild-type (WT). All tubers from one plant were displayed. (b) Comparison of tuber numbers per plant between WT plants and *StbHLH93*-KD and *StbHLH93*-OX lines. $n = 10–12$. (c) Distribution of the weight of tubers of WT plants and *StbHLH93*-KD and *StbHLH93*-OX lines: 0–5, 5–10, 10–15, 15–20, 20–30, and > 30 g. $n = 10–12$. (d) Comparison of tuber yield per plant between WT plants and *StbHLH93*-KD and *StbHLH93*-OX lines. $n = 10–12$. (e, f) Numbers of stolons (e) and swollen stolons (f) of *StbHLH93*-KD, *StbHLH93*-OX, and WT plants for 25 d after the switch to short-day conditions. $n = 5$. Data are means ± SD. The *P*-value indicates statistical significance between the WT plants and *StbHLH93* transgenic lines, as determined by Student's *t*-test. All the data were compared with those of WT plants. The box plots in panels (b, d) show the median (horizontal line) and individual values (black dots).

to TOC/TIC TRANSLOCON complexes and starch biosynthesis were affected by StbHLH93, a few important genes (*TOC159*, *TIC20*, *TIC21*, *AGPL1*, *Bt2*, *SSI SBE1*, and *SBEIII*) were selected, and the samples were collected from subapical regions of the stolons in both *StbHLH93*-KD lines and WT plants. The results showed that there was no difference in the expression levels of these genes between *StbHLH93*-KD lines and the WT plants (Fig. S12a–h), which indicated that the alteration of *StbHLH93* transcript level in tubers did not affect the gene expression of TOC/TIC- and starch biosynthesis. Taken together, these results indicate that stolon- or tuber-specific *StbHLH93* regulates *TIC56* expression in the stolon and tuber.

To investigate the effects of the alteration of *StbHLH93* on the proplastid-to-amyloplast transition, stolon subapical regions from *StbHLH93*-KD, *StbHLH93*-OX, and WT plants were collected 7 d after the switch to SD conditions, and TEM was used to observe plastid development in the cortical regions (Lopez-Juez & Pyke, 2005; Denyer & Pike, 2008; Choi *et al.*, 2021). In WT plants, an average of 2–5 amyloplasts with starch granules were visible in one cell section (Fig. 3b,c,f). The amyloplasts number was significantly lower in the *StbHLH93*-KD lines than in WT plants, and a large number of proplastids remained undifferentiated (Fig. 3b,d,g); by contrast, more proplastids had differentiated into typical mature amyloplasts in *StbHLH93*-OX lines, and amyloplasts number significantly increased compared with WT plants (Fig. 3b,e,h). Taken together, these data indicated that changes in *StbHLH93* expression affect the proplastid-to-amyloplast differentiation process of the stolon-to-tuber transition of potato.

Tic56 affects the stolon-to-tuber transition in potato

Our results indicate that the function of Tic56 may also be linked to the control of the stolon-to-tuber transition. To further assess this, we generated *TIC56*-OX lines driven by the strong 35S promoter and *TIC56*-KD lines driven by the stolon- and tuber-specific *StbHLH93* promoter, which could harness the positive effects of suppressing the *TIC56* gene without collateral negative effects on plant growth. We selected for analysis three independent *TIC56*-KD lines in which *TIC56* expression was reduced to *c.* 35% of the WT level (Fig. S13a), and three independent *TIC56*-OX lines in which *TIC56* expression was increased more than sixfold relative to WT (Fig. S13b). All *TIC56*-KD lines showed that the tuber number and tuber size were significantly reduced, leading to a 39.7% lower tuber yield compared with the

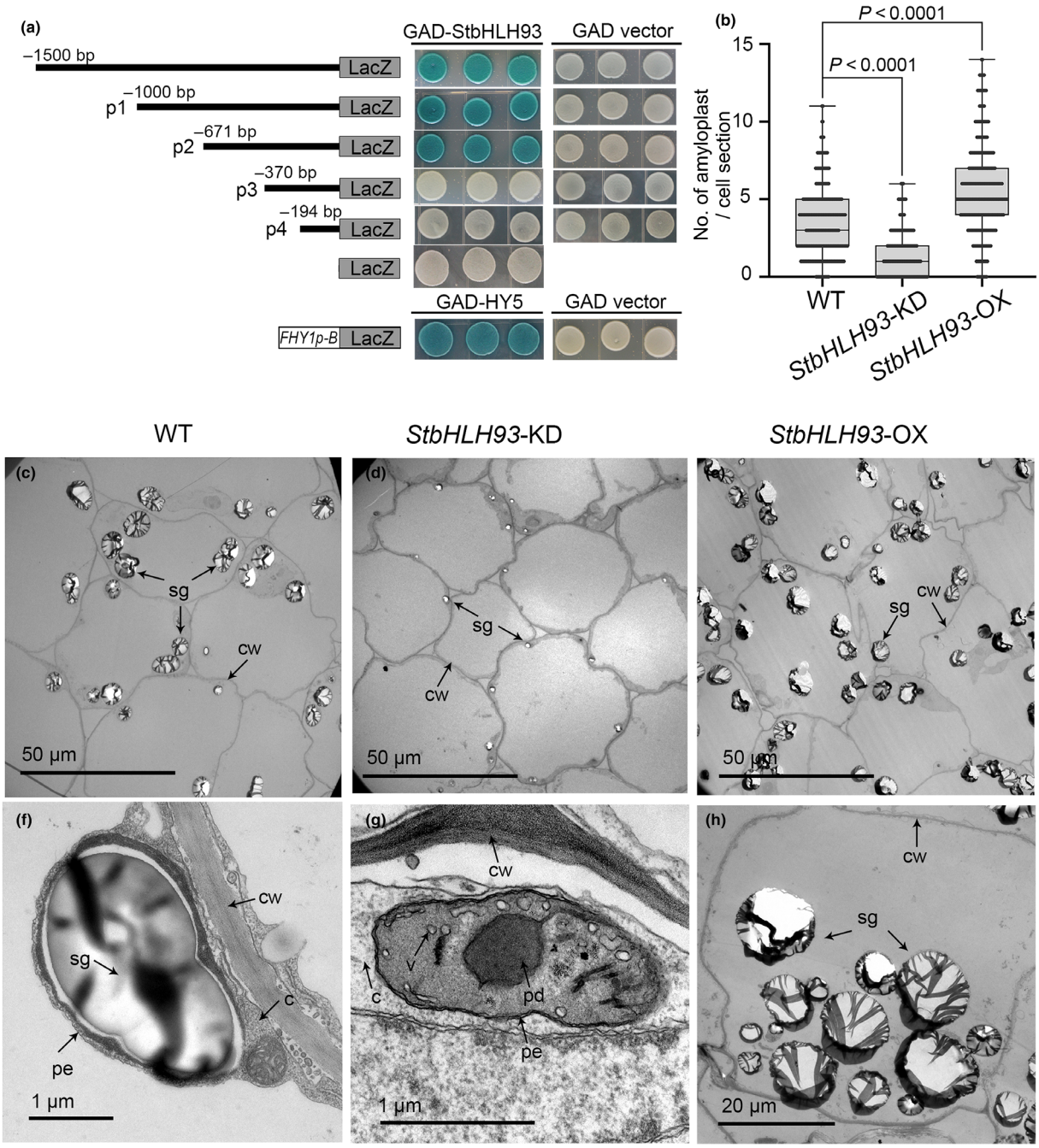

Fig. 3 StbHLH93 binds to the promoter of *TIC56* and regulates the proplastid-to-amyloplast transition in the potato. (a) Diagram of a series fragments of *pro-TIC56* and yeast one-hybrid (Y1H) assay results. The HY5 transcription factor and the *ABI5* promoter from *Arabidopsis* were used as positive controls. The blue stain indicates positive binding. Yeast co-transformed with plasmid GAD-StbHLH9 and empty pLacZi2u vector (*−::LacZ*) as well as with the plasmid GAD and *proTIC56::LacZ* were used as negative controls. (b) Number of amyloplasts per cell section in *StbHLH93*-KD, *StbHLH93*-OX, and wild-type (WT) plants. Samples were collected from subapical regions of stolons 7 d after the plants switch to short-day (SD) conditions. $n = 100–150$. Data are means ± SD. The *P*-value indicates statistical significance between the WT plants and *StbHLH93* transgenic lines, as determined by Student's *t*-test. The box plots show the median (horizontal line) and individual values (black dots). (c–h) Transmission electron microscopy (TEM) depicting amyloplast development in cortex regions of stolon subapical region from WT plants (c), *StbHLH93*-KD (d), and *StbHLH93*-OX (e) lines. Bar, (c–e) 50 μm. Proplastids started to differentiated into amyloplast (f). Proplastids remained undifferentiated in *StbHLH93*-KD lines (g). Proplastids had differentiated into typical mature amyloplasts (h). Bars: (f, g) 1 μm; (h) 20 μm. Samples were collected from subapical regions of stolons 7 d after the plants switch to SD conditions. c, cytosol; cw, cell wall; pd, protein deposit; pe, plastid envelope; sg, starch granule; v, vesicle.

WT plants (Fig. 4a–d), whereas the tuber number, tuber size, and tuber yield were increased in the *TIC56*-OX lines (Figs 4b–d, S14). The tuberization time delayed in *TIC56*-KD lines and accelerated in *TIC56*-OX lines compared with that of WT plants; however, there were no significant differences in stolon number among the *TIC56*-KD, *TIC56*-OX, and WT plants (Fig. 4e,f).

New Phytologist

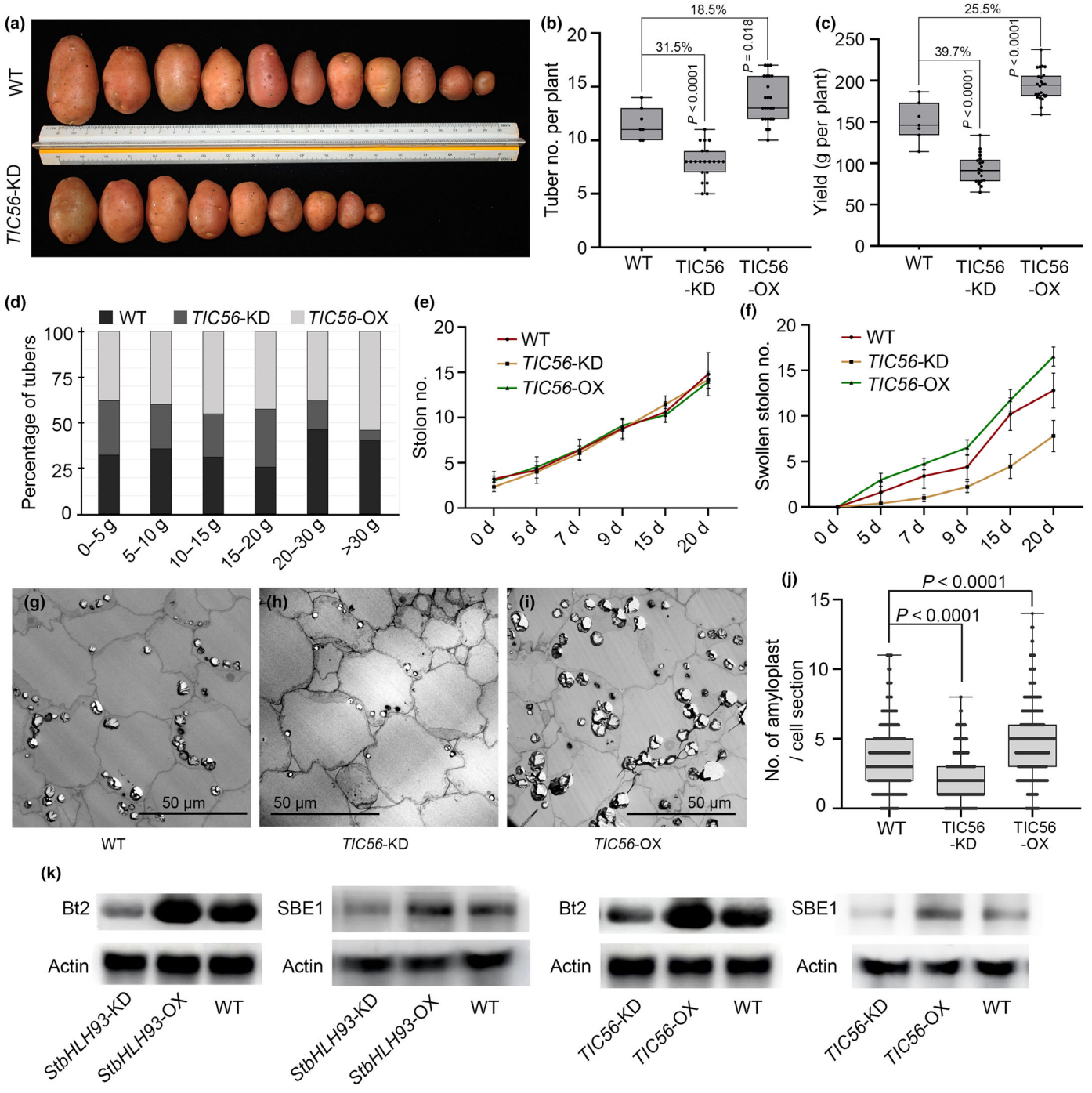

Fig. 4 Phenotypes of potato *TIC56*-KD and *TIC56*-OX transgenic lines. (a) Tuberization phenotype of a representative *TIC56*-KD transgenic plant and wild-type (WT). All tubers from one plant were displayed. (b, c) Comparison of tuber numbers (b) and yield (c) per plant among *TIC56*-KD, *TIC56*-OX, and WT plants. $n = 6$–10. (d) Distribution of the weight of tubers of *TIC56*-KD, *TIC56*-OX, and WT plants: 0–5, 5–10, 10–15, 15–20, 20–30, and > 30 g. $n = 6$–10. (e, f) Numbers of stolons (e) and swollen stolons (f) of *TIC56*-KD, *TIC56*-OX, and WT plants for 25 d after the switch to short-day (SD) conditions. $n = 5$. (g–i) Transmission electron microscopy (TEM) depicting amyloplast development in cortex regions of stolon subapical region from WT plants (g), *TIC56*-KD (h) lines, and *TIC56*-OX lines (i). Bar, 50 μm. (j) Number of amyloplasts per cell section in *TIC56*-KD, *TIC56*-OX, and WT plants. Samples were collected from subapical regions of stolons 7 d after the plants switch to SD conditions. $n = 100$–150. (k) Immunoblotting analysis of total protein extracts from stolon subapical (collected 7 d after the switch to SD conditions) of the different potato genotypes, using ZmBt2, ZmSBE1, and Actin (as a loading control) antibodies. In each case, the protein bands were visualized by chemiluminescence imaging. The data obtained for proteins of interest were normalized relative to corresponding Actin data. Data are means ± SD. The *P*-value indicates statistical significance among the *TIC56*-KD, *TIC56*-OX, and WT plants, as determined by Student's *t*-test. All the data were compared with those of WT plants. The box plots in panels (b, c, j) show the median (horizontal line) and individual values (black dots).

TEM showed that the amyloplasts number of *TIC56*-KD was significantly lower compared with *TIC56*-OX and WT plants (Fig. 4g–j). In addition, a few tuber key regulator genes (*StSP6A*, *StPHYB*, *StCDF1.1*, *StBRC1b*, *StABL1*, and *StSWEET11*) were selected to check the transcript level in both *TIC56*-KD lines and WT plants. We did not observe transcript abundance changes in these genes in *TIC56*-KD lines (Fig. S15a–f), which indicated that the alteration of *TIC56* transcript level in tuber did not affect the gene expression of tuberization-related key genes. Overall, these data were in agreement with our hypothesis on Tic56 function in potato, thus supporting the role of Tic56 in facilitating the stolon-to-tuber transition in potato.

To better understand the links between plastid proteome changes and the differentiation of the amyloplast, protein extracts from stolon subapical (collected 7 d after the switch to SD conditions) of the different potato genotypes were analyzed by immunoblotting (Kahlau & Bock, 2008; Kakizaki *et al.*, 2009). The data showed that the abundance of amyloplast enzymes Bt2 and SBE1 was strongly elevated in *StbHLH93*-OX and *TIC56*-OX transgenic plants relative to WT and significantly reduced in *StbHLH93*-KD and *TIC56*-KD transgenic plants (Fig. 4k). These results supported that StbHLH93 and Tic56 regulate potato plastid protein levels during plastid transitions.

Discussion

Gene co-expression modules inform cellular processes during stolon and tuber development

In potato, tuber number and size are determinants of potato yield and are directly affected by stolon swelling. Thus, it is critical to understand the mechanism underlying the stolon-to-tuber transition and tuber development. However, to date, only a few key genes related to tuber swelling have been identified, and little is known about the global gene expression network (Dutt *et al.*, 2017; Hannapel *et al.*, 2017; Zierer *et al.*, 2021). In this study, we profiled mRNAs throughout stolon swelling and tuber development to identify key genes and to understand the processes of the stolon-to-tuber transition.

Our analysis identified 20 545 genes that are important for tuber development. The results of hierarchical clustering and PCA clearly showed that the tuberization process could be divided into four main development phases: stolon noninduction (stage 1), stolon induction (stage 2), stolon swelling (stage 3), and tuber development (stages 4–8; Fig. Sa,b). Gene expression pattern analysis showed that the genes belonging to the first five co-expressed clusters (clusters I–IV) were mainly expressed during the four developmental phases and represented a particular function for the corresponding phases (Fig. 1b). In the noninduced stolon phase, the genes were mainly related to phytohormone signal transduction and photosynthesis. For the photosynthetic genes, they were photosystem I (PSI), PSII, and chlorophyll a/b-binding protein. This was also observed in rice, pea, and *Arabidopsis* that nuclear photosynthetic genes were expressed in root at the absence of light (Sullivan & Gray, 1999; Moumeni *et al.*, 2011; Minh-Thu *et al.*, 2013). After the photoperiod was switched from LD to SD, many genes involved in biological ROS processes were expressed; however, in the swelling stolon phase, genes were mainly enriched in plastid biogenesis, and in the tuber development phase, genes were mainly enriched in the biological process of carbohydrate accumulation (Fig. S2). These results indicated that gene co-expression modules inform different cellular processes during stolon and tuber development.

At least 56% of the total genes (clusters II and III) were detected during the stolon-to-tuber transition, indicating that this transition is one of the major events of potato formation (Fig. 1b). The expression of the genes in cluster III increased from stage 1 to stage 3 and was low expression at later time points, which is consistent with the process of stolon-to-tuber transition (Fig. 1b). Furthermore, 63.17% (494/782) of the stolon- and tuber-specific expressed genes were also assigned to cluster III gene sets (Fig. S3), indicating the important role of this co-expressed gene set in the stolon-to-tuber transition. Together, these data constitute a rich resource for determining the underlying mechanisms of potato tuberization. Of the 494 stolon- and tuber-specific genes, only one gene encoded a bHLH TF protein, which was highly expressed in the apical meristem and perimedullary zone during the stolon-to-tuber transition process (Fig.1d,e). Previous studies have shown that the bHLH family plays an important role in cell fate determination and tissue differentiation in plants (Feller *et al.*, 2011; Hao *et al.*, 2021; Zhang *et al.*, 2021), suggesting that this bHLH TF has a potentially critical role in potato tuberization.

The stolon-to-tuber transition in potato is associated with the proplastid-to-amyloplast development

Stolon-to-tuber transition is the most striking feature of potato plants. This transition requires specific genetic programs that respond to specific positional and environmental cues. We propose that the tuber-specific TF *StbHLH93* may play a critical role in the stolon-to-tuber transition. To investigate the function of tuber-specific TFs, in this study, *StbHLH93*-KD and *StbHLH93*-OX transgenic plants were generated, and fewer and smaller tubers were produced by the *StbHLH93*-KD lines than by the WT plants, resulting in a significant reduction in total tuber yield (Fig. 2a–d). Conversely, *StbHLH93*-OX lines exhibited an enhanced tuber number per plant and an increased tuber weight, resulting in yield increase compared with the WT (Figs 2b–d, S8). In addition, there was no significant difference in the aboveground phenotypes, including plant height, leaf size, and color, among the *StbHLH93*-KD, *StbHLH93*-OX, and WT plants (Fig. S7a–c). To further explore the mechanisms underlying the fewer and smaller tuber phenotypes of the *StbHLH93*-KD lines, we investigated stolon tuberization for 25 d after the plants were switched to SD conditions, and no significant difference in stolon number was observed among *StbHLH93*-KD, *StbHLH93*-OX, and WT plants. However, the initiation of stolon swelling was delayed in the *StbHLH93*-KD lines and accelerated in *StbHLH93*-OX, relative to WT, leading to the number of swollen stolons significantly increased in *StbHLH93*-OX lines,

while it decreased noticeably in *StbHLH93*-KD lines (Fig. 2e,f). These results indicated that *StbHLH93* is critical for stolon swelling in potato and that a deficiency in this gene leads to problematic stolon swelling.

To further understand the StbHLH93-related regulatory network, we found that StbHLH93 could bind to the *TIC56* promoter and positively regulate its expression (Fig. 3a). Tic56 is a component of the TRANSLOCON complexes in the inner chloroplast envelope membrane, and previous studies have shown that *tic56* mutants exhibit abnormal chloroplast and leaf development (Köhler *et al.*, 2015, 2016). Thus, we further investigated plastid development and found that a large number of proplastids remained undifferentiated at the stolon swelling stage in the *StbHLH93*-KD lines compared with the WT plants (Fig. 3d,g). The *TIC56*-KD lines driven by the stolon- and tuber-specific *StbHLH93* promoter and *TIC56*-OX lines driven by the strong 35S promoter were also generated, which showed a phenotype similar to *StbHLH93*-KD and *StbHLH93*-OX lines, and the number of amyloplasts was significantly reduced in the *TIC56*-KD and increased in *TIC56*-OX lines compared with WT plants (Fig. 4g–j). In addition, TICs were shown to tightly co-regulate plastid protein import (Jarvis & Lopez-Juez, 2013); however, there were no significant changes in the expression levels of TOC/TIC and key starch biosynthesis-related genes (*TOC159*, *TIC20*, *TIC21*, *AGPL1*, *Bt2*, *SSI*, *SBE1*, and *SBEIII*) between the *StbHLH93*-KD lines and WT plants (Fig. S12), suggesting that *StbHLH93* activates *TIC56* to affect proplastid-to-amyloplast differentiation during tuberization. A few studies have reported that Tic56 deficiency affects rRNA processing and ribosome assembly and disturbs plastid development, causing an albino phenotype (Köhler *et al.*, 2015, 2016). In line with the results of our transcriptomic analysis, a large number of genes were enriched in the ribosome biogenesis pathways during stolon swelling (Fig. S2), which might indicate that Tic56 functions in potato stolon swelling by affecting plastid rRNA processing. To better understand the links between plastid protein levels and the differentiation of the amyloplast, the immunoblotting analysis was performed and showed that StbHLH93 and Tic56 regulate potato plastid protein levels during plastid transitions (Fig. 4k).

Plastids are an important group of major organelles in plant cells and are essential components of plant cell functions (Neuhaus & Emes, 2000; Lopez-Juez & Pyke, 2005). Plastids constitute a family of structurally and functionally diverse organelles with many important biological functions (Kode *et al.*, 2005; Inaba & Ito-Inaba, 2010; Karlova *et al.*, 2011; Romani *et al.*, 2012; Leister & Kleine, 2016; Duan *et al.*, 2020). The phenotypes of *TIC56*-KD and *TIC56*-OX lines indicated that Tic56 is linked to the control of the stolon-to-tuber transition (Fig. 4). However, there were no significant changes in the expression levels of tuber key regulator genes (*StSP6A*, *StPHYB*, *StCDF1.1*, *StBRC1b*, *StABL1*, and *StSWEET11*) between the *TIC56*-KD lines and WT plants (Fig. S15). Immunoblotting analysis shows that the abundance of amyloplast enzymes Bt2 and SBE1 was elevated in *StbHLH93*-OX and *TIC56*-OX, and reduced in *StbHLH93*-KD and *TIC56*-KD, while the expression level of *Bt2* and *SBE1* did not show significant changes in *StbHLH93*-OX compared with the WT (Figs 4k, S12e,f). These results suggested that *StbHLH93* regulates amyloplast differentiation through plastid proteome changes rather than through gene expression. In the future, it will be interesting to analyze a greater range of signals and pathways, to better understand the anterograde and retrograde signaling, to more fully appreciate the link between plastid differentiation and stolon swelling in potato. Overall, we identified a new tuber-specific TF *StbHLH93* that activates plastid protein import system gene *TIC56* expression to mediate stolon swelling by facilitating proplastid-to-amyloplast differentiation. We conclude that proplastid-to-amyloplast differentiation plays vital roles in the stolon-to-tuber transition during potato tuberization (Fig. 5).

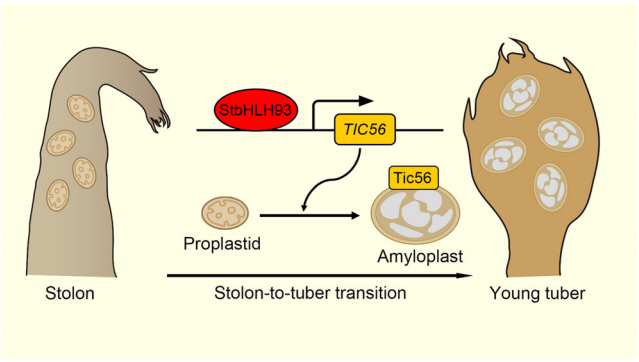

Fig. 5 Model through which StbHLH93 regulates amyloplast development to affect stolon swelling in potato. Under short-day conditions, StbHLH93 accumulates in the stolon apical tip, binding the promoter region of *TIC56* and activates the expression of *TIC56* to initiate proplastid-to-amyloplast differentiation, eventually inducing stolon swelling.

Acknowledgements

This work was supported by the National Natural Science Foundation of China (grant no. 31972969); Science and Technology Department of Yunnan Province (grant no. 2019FY003015); Research Startup Funding of Yunnan University in China (grant no. C176220100033); Science and Technology Major Project of Department of Science and Technology of Yunnan (grant no. K204204210017); Yunnan Fundamental Research Projects (grant no. 202301BF070001-026); and China Postdoctoral Science Foundation (grant no. 2020M673311).

Competing interests

None declared.

Author contributions

RY and BH designed the research and wrote the paper. RY, YS, XZ, BJ, SS, YC, LL, XW and QZ performed the research. BJ, YC, LL, XW and QZ contributed new reagents/analytic tools. RY, YS, XZ, BJ, QL and BH analyzed the data. RY, YS and XZ contributed equally to this work.

ORCID

Binquan Huang https://orcid.org/0000-0003-3267-0343
Baozhen Jiao https://orcid.org/0009-0001-7332-1783
Sifan Sun https://orcid.org/0000-0001-5840-3249
Yuan Sun https://orcid.org/0009-0009-4512-7957
Rui Yang https://orcid.org/0009-0008-7487-7880
Xiaoling Zhu https://orcid.org/0000-0003-4544-8768

Data availability

The data that support the findings of this study are available in the Supporting Information of this article. The RNA-Seq data are available in the NCBI Sequence Read Archive under accession no. PRJNA943592.

References

Abelenda JA, Bergonzi S, Oortwijn M, Sonnewald S, Du M, Visser RGF, Sonnewald U, Bachem CWB. 2019. Source-sink regulation is mediated by interaction of an FT homolog with a SWEET protein in potato. *Current Biology* **29**: 1178–1186.

Abelenda JA, Prat S. 2013. Cytokinins: determinants of sink storage ability. *Current Biology* **23**: R561–R563.

Bhogale S, Mahajan AS, Natarajan B, Rajabhoj M, Thulasiram HV, Banerjee AK. 2014. MicroRNA156: a potential graft-transmissible microRNA that modulates plant architecture and tuberization in *Solanum tuberosum* ssp. *andigena*. *Plant Physiology* **164**: 1011–1027.

Brosch M, Krause K, Falk J, Krupinska K. 2007. Analysis of gene expression in amyloplasts of potato tubers. *Planta* **227**: 91–99.

Chincinska I, Gier K, Krügel U, Liesche J, He H, Grimm B, Harren FJ, Cristescu SM, Kühn C. 2013. Photoperiodic regulation of the sucrose transporter StSUT4 affects the expression of circadian-regulated genes and ethylene production. *Frontiers in Plant Science* **4**: 26.

Choi H, Yi T, Ha SH. 2021. Diversity of plastid types and their interconversions. *Frontiers in Plant Science* **12**: 692024.

Denyer K, Pike M. 2008. Isolation of amyloplasts. *Current Protocols in Cell Biology* Chapter 3: Unit 3.28.

Duan S, Hu L, Dong B, Jin HL, Wang HB. 2020. Signaling from plastid genome stability modulates endoreplication and cell cycle during plant development. *Cell Reports* **32**: 108019.

Dutt S, Manjul AS, Raigond P, Singh B, Siddappa S, Bhardwaj V, Kawar PG, Patil VU, Kardile HB. 2017. Key players associated with tuberization in potato: potential candidates for genetic engineering. *Critical Reviews in Biotechnology* **37**: 942–957.

Faith JJ, Hayete B, Thaden JT, Mogno I, Wierzbowski J, Cottarel G, Kasif S, Collins JJ, Gardner TS. 2007. Large-scale mapping and validation of *Escherichia coli* transcriptional regulation from a compendium of expression profiles. *PLoS Biology* **5**: e8.

Feller A, Machemer K, Braun EL, Grotewold E. 2011. Evolutionary and comparative analysis of MYB and bHLH plant transcription factors. *The Plant Journal* **66**: 94–116.

Hancock RD, Morris WL, Ducreux LJ, Morris JA, Usman M, Verrall SR, Fuller J, Simpson CG, Zhang R, Hedley PE *et al.* 2014. Physiological, biochemical and molecular responses of the potato (*Solanum tuberosum* L.) plant to moderately elevated temperature. *Plant, Cell & Environment* **37**: 439–450.

Hannapel DJ, Sharma P, Lin T, Banerjee AK. 2017. The multiple signals that control tuber formation. *Plant Physiology* **174**: 845–856.

Hao Y, Zong X, Ren P, Qian Y, Fu A. 2021. Basic helix-loop-helix (bHLH) transcription factors regulate a wide range of functions in *Arabidopsis*. *International Journal of Molecular Sciences* **22**: 7152.

Hayward A, Stirnberg P, Beveridge C, Leyser O. 2009. Interactions between auxin and strigolactone in shoot branching control. *Plant Physiology* **151**: 400–412.

Inaba T, Ito-Inaba Y. 2010. Versatile roles of plastids in plant growth and development. *Plant Cell Physiology* **51**: 1847–1853.

Jackson SD, James P, Prat S, Thomas B. 1998. Phytochrome B affects the levels of a graft-transmissible signal involved in tuberization. *Plant Physiology* **117**: 29–32.

Jarvis P, Lopez-Juez E. 2013. Biogenesis and homeostasis of chloroplasts and other plastids. *Nature Reviews Molecular Cell Biology* **14**: 787–802.

Jing S, Sun X, Yu L, Wang E, Cheng Z, Liu H, Jiang P, Qin J, Begum S, Song B. 2022. Transcription factor StABI5-like 1 binding to the FLOWERING LOCUS T homologs promotes early maturity in potato. *Plant Physiology* **189**: 1677–1693.

Kahlau S, Bock R. 2008. Plastid transcriptomics and translatomics of tomato fruit development and chloroplast-to-chromoplast differentiation: chromoplast gene expression largely serves the production of a single protein. *Plant Cell* **20**: 856–874.

Kakizaki T, Matsumura H, Nakayama K, Che FS, Terauchi R, Inaba T. 2009. Coordination of plastid protein import and nuclear gene expression by plastid-to-nucleus retrograde signaling. *Plant Physiology* **151**: 1339–1353.

Karlova R, Rosin FM, Busscher-Lange J, Parapunova V, Do PT, Fernie AR, Fraser PD, Baxter C, Angenent GC, de Maagd RA. 2011. Transcriptome and metabolite profiling show that APETALA2a is a major regulator of tomato fruit ripening. *Plant Cell* **23**: 923–941.

Kloosterman B, Abelenda JA, Gomez Mdel M, Oortwijn M, de Boer JM, Kowitwanich K, Horvath BM, van Eck HJ, Smaczniak C, Prat S *et al.* 2013. Naturally occurring allele diversity allows potato cultivation in northern latitudes. *Nature* **495**: 246–250.

Kloosterman B, Vorst O, Hall RD, Visser RG, Bachem CW. 2005. Tuber on a chip: differential gene expression during potato tuber development. *Plant Biotechnology Journal* **5**: 505–519.

Kode V, Mudd EA, Iamtham S, Day A. 2005. The tobacco plastid accD gene is essential and is required for leaf development. *The Plant Journal* **44**: 237–244.

Köhler D, Helm S, Agne B, Baginsky S. 2016. Importance of translocon subunit Tic56 for rRNA processing and chloroplast ribosome assembly. *Plant Physiology* **172**: 2429–2444.

Köhler D, Montandon C, Hause G, Majovsky P, Kessler F, Baginsky S, Agne B. 2015. Characterization of chloroplast protein import without Tic56, a component of the 1-megadalton translocon at the inner envelope membrane of chloroplasts. *Plant Physiology* **167**: 972–990.

Kondhare KR, Kumar A, Patil NS, Malankar NN, Saha K, Banerjee AK. 2021a. Development of aerial and belowground tubers in potato is governed by photoperiod and epigenetic mechanism. *Plant Physiology* **187**: 1071–1086.

Kondhare KR, Patil AB, Giri AP. 2021b. Auxin: an emerging regulator of tuber and storage root development. *Plant Science* **306**: 110854.

Leister D, Kleine T. 2016. Definition of a core module for the nuclear retrograde response to altered organellar gene expression identifies GLK overexpressors as gun mutants. *Physiologia Plantarum* **157**: 297–309.

Li J, Li G, Gao S, Martinez C, He G, Zhou Z, Huang X, Lee JH, Zhang H, Shen Y *et al.* 2010. *Arabidopsis* transcription factor ELONGATED HYPOCOTYL5 plays a role in the feedback regulation of phytochrome A signaling. *Plant Cell* **22**: 3634–3649.

Lin T, Sharma P, Gonzalez DH, Viola IL, Hannapel DJ. 2013. The impact of the long-distance transport of a BEL1-like messenger RNA on development. *Plant Physiology* **161**: 760–772.

Lopez-Juez E, Pyke KA. 2005. Plastids unleashed: their development and their integration in plant development. *The International Journal of Developmental Biology* **49**: 557–577.

Martin A, Adam H, Diaz-Mendoza M, Zurczak M, Gonzalez-Schain ND, Suarez-Lopez P. 2009. Graft-transmissible induction of potato tuberization by the microRNA miR172. *Development* **136**: 2873–2881.

Millam S. 2006. Potato (*Solanum tuberosum L.*) *Methods. Molecular Biology* **344**: 25–36.

Minh-Thu PT, Hwang DJ, Jeon JS, Nahm BH, Kim YK. 2013. Transcriptome analysis of leaf and root of rice seedling to acute dehydration. *Rice* **6**: 38.

Moumeni A, Satoh K, Kondoh H, Asano T, Hosaka A, Venuprasad R, Serraj R, Kumar A, Leung H, Kikuchi S. 2011. Comparative analysis of root transcriptome profiles of two pairs of drought-tolerant and susceptible rice near-isogenic lines under different drought stress. *BMC Plant Biology* **11**: 174.

Navarro C, Abelenda JA, Cruz-Oró E, Cuéllar CA, Tamaki S, Silva J, Shimamoto K, Prat S. 2011. Control of flowering and storage organ formation in potato by FLOWERING LOCUS T. *Nature* **478**: 119–122.

Neuhaus HE, Emes MJ. 2000. Nonphotosynthetic metabolism in plastids. *Annual Review of Plant Physiology and Plant Molecular Biology* **51**: 111–140.

Nicolas M, Torres-Pérez R, Wahl V, Cruz-Oró E, Rodríguez-Buey ML, Zamarreño AM, Martín-Jouve B, García-Mina JM, Oliveros JC, Prat S *et al.* 2022. Spatial control of potato tuberization by the TCP transcription factor BRANCHED1b. *Nature Plants* **8**: 281–294.

Park JS, Park SJ, Kwon SY, Shin AY, Moon KB, Park JM, Cho HS, Park SU, Jeon JH, Kim HS *et al.* 2022. Temporally distinct regulatory pathways coordinate thermo-responsive storage organ formation in potato. *Cell Reports* **38**: 110579.

Pasare SA, Ducreux LJM, Morris WL, Campbell R, Sharma SK, Roumeliotis E, Kohlen W, van der Krol S, Bramley PM, Roberts AG *et al.* 2013. The role of the potato (*Solanum tuberosum*) CCD8 gene in stolon and tuber development. *New Phytologist* **198**: 1108–1120.

Potato Genome Sequencing Consortium. 2011. Genome sequence and analysis of the tuber crop potato. *Nature* **475**: 189–195.

Romani I, Tadini L, Rossi F, Masiero S, Pribil M, Jahns P, Kater M, Leister D, Pesaresi P. 2012. Versatile roles of *Arabidopsis* plastid ribosomal proteins in plant growth and development. *The Plant Journal* **72**: 922–934.

Roumeliotis E, Visser RG, Bachem CW. 2012. A crosstalk of auxin and GA during tuber development. *Plant Signaling & Behavior* **7**: 1360–1363.

Sakamoto W, Miyagishima SY, Jarvis P. 2008. Chloroplast biogenesis: control of plastid development, protein import, division and inheritance. *The Arabidopsis Book* **6**: e0110.

Singh A, Siddappa S, Bhardwaj V, Singh B, Kumar D, Singh BP. 2015. Expression profiling of potato cultivars with contrasting tuberization at elevated temperature using microarray analysis. *Plant Physiology and Biochemistry* **97**: 108–116.

Spooner DM, Ghislain M, Simon R, Jansky SH, Gavrilenko T. 2014. Systematics, diversity, genetics, and evolution of wild and cultivated potatoes. *Botanical Review* **80**: 283–383.

Stensballe A, Hald S, Bauw G, Blennow A, Welinder KG. 2008. The amyloplast proteome of potato tuber. *FEBS Journal* **275**: 1723–1741.

Sullivan JA, Gray JC. 1999. Plastid translation is required for the expression of nuclear photosynthesis genes in the dark and in roots of the pea lip1 mutant. *Plant Cell* **11**: 901–910.

Tang D, Jia Y, Zhang J, Li H, Cheng L, Wang P, Bao Z, Liu Z, Feng S, Zhu X *et al.* 2022. Genome evolution and diversity of wild and cultivated potatoes. *Nature* **606**: 535–541.

Thomson SM, Pulido P, Jarvis RP. 2020. Protein import into chloroplasts and its regulation by the ubiquitin-proteasome system. *Biochemical Society Transactions* **48**: 71–82.

Xiong W, Wang C, Zhang X, Yang Q, Shao R, Lai J, Du C. 2017. Highly interwoven communities of a gene regulatory network unveil topologically important genes for maize seed development. *The Plant Journal* **92**: 1143–1156.

Xu X, Dick V, Lammeren AMV. 1998. Cell division and cell enlargement during potato tuber formation. *Journal of Experimental Botany* **49**: 573–582.

Yang H, Li Y, Cao Y, Shi W, Xie E, Mu N, Du G, Shen Y, Tang D, Cheng Z *et al.* 2022. Nitrogen nutrition contributes to plant fertility by affecting meiosis initiation. *Nature Communications* **13**: 485.

Yi F, Gu W, Chen J, Song N, Gao X, Zhang X, Zhou Y, Ma X, Song W, Zhao H *et al.* 2019. High temporal-resolution transcriptome landscape of early maize seed development. *Plant Cell* **31**: 974–992.

Zhang Y, Mitsuda N, Yoshizumi T, Horii Y, Oshima Y, Ohme-Takagi M, Matsui M, Kakimoto T. 2021. Two types of bHLH transcription factor determine the competence of the pericycle for lateral root initiation. *Nature Plants* **7**: 633–643.

Zhuang K, Kong F, Zhang S, Meng C, Yang M, Liu Z, Wang Y, Ma N, Meng Q. 2019. Whirly1 enhances tolerance to chilling stress in tomato via protection of photosystem II and regulation of starch degradation. *New Phytologist* **221**: 1998–2012.

Zierer W, Ruscher D, Sonnewald U, Sonnewald S. 2021. Tuber and tuberous root development. *Annual Review of Plant Biology* **72**: 551–580.

Supporting Information

Additional Supporting Information may be found online in the Supporting Information section at the end of the article.

Fig. S1 Transcriptomic relationships among eight developmental stages of potato tubers.

Fig. S2 Gene functional transition over the time course.

Fig. S3 Expression patterns and functional enrichment of stolon- and tuber-specific genes (including transcription factors) at different developmental stages.

Fig. S4 Transmission electron microscopy analysis of tuber development.

Fig. S5 Real-time qPCR analysis of *StbHLH93* expression levels in various tissues and in developing tubers of Désirée.

Fig. S6 Transcript levels of *StbHLH93* in wild-type plants, *StbHLH93*-KD and *StbHLH93*-OX lines.

Fig. S7 Aboveground phenotypes of potato *StbHLH93* transgenic lines and wild-type plant.

Fig. S8 Tuberization phenotype of a representative *StbHLH93*-OX transgenic plant and wild-type plant.

Fig. S9 Yeast one-hybrid assay results of predicted transcription factor-encoding gene regulation.

Fig. S10 Luciferase activation assay of StbHLH93-*proTIC56* regulation.

Fig. S11 Comparison of the relative expression levels of *TIC56*.

Fig. S12 Analyses of the effects of *StbHLH93* on starch synthesis- and TRANSLOCON complex-related gene expression.

Fig. S13 Transcript levels of *TIC56* in wild-type plants, *TIC56*-KD and *TIC56*-OX lines.

Fig. S14 Tuberization phenotype of a representative *TIC56*-KD transgenic plant and wild-type.

Fig. S15 Analyses of the effects of *TIC56* on tuber regulator gene expression.

Table S1 Primers used in this study.

Table S2 Gene expression levels at eight different developmental stages of potato tubers.

Table S3 Top 10 target genes of *StbHLH93* with the most connections in the gene regulatory network.

Please note: Wiley is not responsible for the content or functionality of any Supporting Information supplied by the authors. Any queries (other than missing material) should be directed to the *New Phytologist* Central Office.